Supporting Information

Welcoming natural isotopic abundance in solid-state NMR: probing π-stacking and supramolecular structure of organic nanoassemblies using DNP

Katharina Märker,ϟ[ab] Subhradip Paul,ϟ‖[ab] Carlos Fernández-de-Alba,[ab] Daniel Lee,[ab] Jean-Marie Mouesca,[ab] Sabine Hediger,[abc] Gaël De Paëpe*[ab]

[a]Univ. Grenoble Alpes, INAC, F-38000 Grenoble, France.

[b]CEA, INAC, F-38000 Grenoble, France.

[c]CNRS, MEM, F-38000 Grenoble, France.

ϟ These authors contributed equally to this work.

‖ Present address: Sir Peter Mansfield Imaging Centre, Department of Physics and Astronomy, University of Nottingham, NG72RD, UK.

Contents

1) DFT-GIPAW results on the cyclo-FF crystal structure

Table S1 Experimental chemical shifts and calculated chemical shielding tensor properties for cyclo-FF from GIPAW[1] computations with Quantum ESPRESSO,[2] obtained after optimization of hydrogen positions in the crystal structure.[3]

	δ_{expt} [a]	σ_{xx} [b]	σ_{yy} [b]	σ_{zz} [b]	σ_{iso} [b]	σ_{aniso} [b]	η [b]
CO[1]	169.3	-77.4	-20.6	84.8	-4.4	133.8	0.64
CO[2]	168.4	-74.9	-25.7	86.3	-4.8	136.6	0.54
Cγ$_1$	137.4	-76.7	-13.5	159.6	23.1	204.6	0.46
Cγ$_2$	135.8	-76.8	-11.3	160.9	24.3	204.9	0.48
Cδ$_{21}$	132.9	-75.9	13.9	149.8	29.3	180.8	0.75
Cδ$_1$	130.9	-73.3	15.8	151.4	31.3	180.1	0.74
Cδ$_1$	130.9	-76.7	18.6	149.1	30.3	178.1	0.80
Cϵ$_{21}$	130.4	-77.4	12.0	160.4	31.7	193.1	0.69
Cδ$_{22}$	129.9	-74.3	18.9	150.6	31.7	178.3	0.78
Cϵ$_1$	129.6	-78.6	10.4	162.8	31.5	196.9	0.68
Cϵ$_1$	129.6	-77.7	13.3	160.3	32.0	192.5	0.71
Cϵ$_{22}$	128.4	-75.0	14.9	160.4	33.4	190.5	0.71
Cζ$_1$	126.5	-73.9	18.0	163.1	35.7	191.0	0.72
Cζ$_2$	125.9	-75.2	19.3	163.6	35.9	191.6	0.74
Cα$_1$	56.2	94.0	103.7	122.1	106.6	23.2	0.63
Cα$_2$	55.5	124.6	110.7	88.1	107.8	-29.5	0.71
Cβ$_1$	43.8	112.9	116.3	125.0	118.1	10.4	0.48
Cβ$_2$	39.1	113.7	121.6	135.2	123.5	17.5	0.68

[a] Experimental chemical shifts (δ_{expt}) are referenced with respect to the CO of glycine at room temperature (176.0 ppm). [b] Chemical shift tensor properties are given according to the Haeberlen convention[4] with $|\sigma_{zz} - \sigma_{iso}| \geq |\sigma_{xx} - \sigma_{iso}| \geq |\sigma_{yy} - \sigma_{iso}|$, $\sigma_{iso} = 1/3\,(\sigma_{xx} + \sigma_{yy} + \sigma_{zz})$, $\sigma_{aniso} = \sigma_{zz} - \sigma_{iso}$ and $\eta = (\sigma_{yy} - \sigma_{xx})/\sigma_{aniso}$.

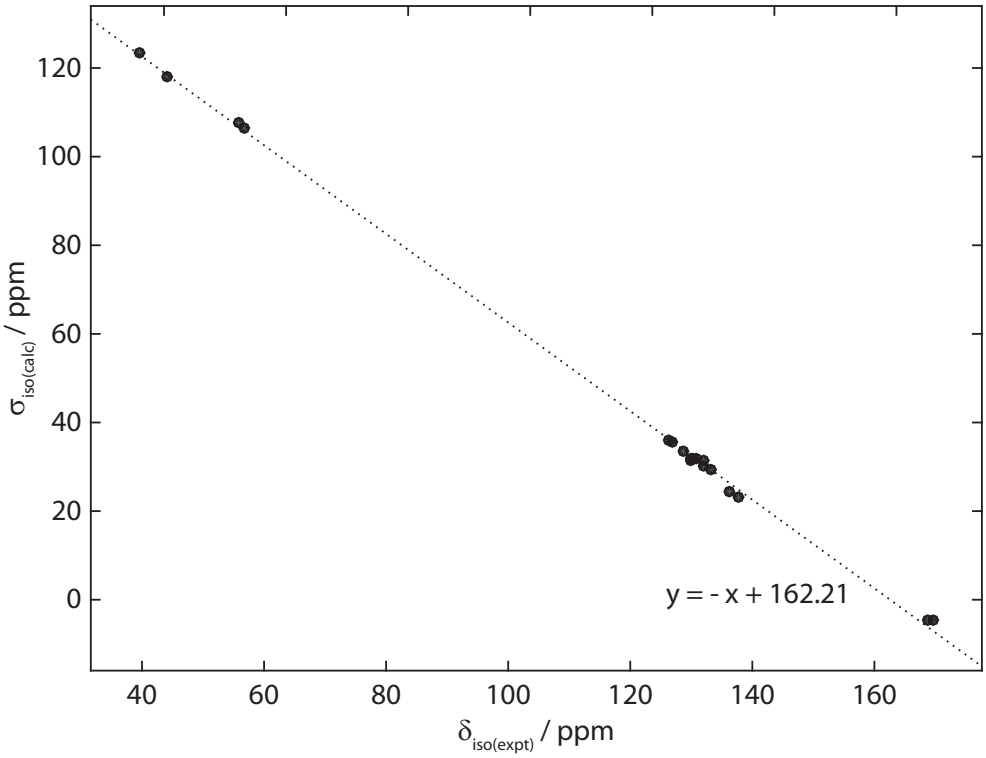

Fig. S1 Comparison of calculated isotropic chemical shielding constants ($\sigma_{iso(calc)}$) and experimental isotropic chemical shifts ($\delta_{iso(expt)}$) of cyclo-FF. A straight line fit is shown as dotted line and its equation is given. After referencing the calculated shielding constants with respect to this equation ($\delta_{iso(calc)} = - \sigma_{iso(calc)} + 162.21$), a root mean square deviation of 1.09 ppm is obtained when comparing calculated and experimental isotropic chemical shifts.

2) Experimental details on the acquisition of polarization buildup curves

General conditions for DNP-enhanced ssNMR experiments

All DNP experiments were performed on a wide-bore AVIII 400 MHz (^{1}H Larmor frequency) Bruker DNP-NMR spectrometer equipped with a 263 GHz gyrotron, a μw transmission line and a low temperature 3.2 mm MAS-DNP probe in double-resonance mode operating at ~105 K. All spectra were recorded at a MAS frequency of 13.889 kHz with a recycle delay of 6.5 s. Data were recorded using Bruker Topspin 3.2 software. 1D spectra were processed with Topspin while the 2Ds were processed with NMRPipe.[5] Chemical shifts were referenced with respect to TMS at 0 ppm using the CO resonance of glycine at room temperature (176.0 ppm) as an external reference. Proton and carbon π/2 pulses were applied at 100 kHz and 50 kHz RF-field strength, respectively. For CP from proton to carbon, the ^{13}C RF-field strength was fixed to 48 kHz and a linear ramp from 80 to 100 % was applied on the proton channel, with the maximum ^{1}H RF-field strength at 72 kHz. The CP contact time was 3 ms. Pre-saturation pulse trains were applied on both the proton and carbon channel prior to experiments.

1D spectra for the measurement of CO to aromatics polarization buildups

The 1D spectra for buildup analysis were acquired with the pulse sequence shown in Fig. 2a. All carbon pulses except the soft pulses were centered between the carbonyl and aromatic resonances (153 ppm). Both continuous-wave (CW)[6] and SPINAL-64 heteronuclear decoupling[7] were applied at 100 kHz RF-field strength. After CP, a ^{13}C 270° Gaussian pulse (truncated at 1%) of 2.5 ms length and centered on the CO resonances (169 ppm) was applied to selectively flip up the carbonyl spins. Remaining transversal carbon magnetization was left to decay for 1 ms, assisted by a low-power purge pulse centered on the aromatic resonances (129 ppm) and applied at an RF-field strength of ~0.38 kHz. [S_3] homonuclear recoupling[8] was then applied, with the π/2 bracketing pulses and the S_3 pulses at RF-field strengths of 50 kHz and 6.9 kHz, respectively. To measure the polarization buildups, 15 different mixing times were used, taking into account between 1 and 20 loops of S_3 between the bracketing pulses, with 1 loop of S_3 spanning 16 rotor cycles (1.152 ms in total). After the recoupling period, a *z*-filter of 100 μs was applied, followed by a selective E-BURP2[9] pulse centered on the aromatic carbons (129 ppm) and applied at an average RF-field strength of 2.48 kHz with a duration of 1.65 ms. The acquisition time was 25 ms. For each mixing time, 256 transients were accumulated, corresponding to ~28 min per spectrum, leading to a total experimental time of ~7 h for the whole set of 1D spectra. Spectra were processed without any apodization. The aromatic region of each spectrum was deconvoluted using simplex algorithm with Topspin to determine the peak integrals of $C\gamma_1$, $C\gamma_2$, $C\delta_{21}$, $C\epsilon_{22}$, $C\zeta_1$, and $C\zeta_2$.

Normalization of peak integrals in 1D buildups

For a better comparison to simulations, the peak integrals from the 1D spectra described above were normalized according to the initial polarization on CO spins. For this purpose, a reference experiment was performed replacing the entire recoupling block by a π/2 ^{13}C excitation pulse with subsequent detection. The integral of the CO peak was then divided by 2 (owing to the presence of 2 COs per molecule), and multiplied by 0.011 to take into account the probability of finding a particular ^{13}C spin in proximity to one of the ^{13}CO in NA cyclo-FF. This scaled CO-integral was then used as normalization factor for all integrals of the aromatic resonances. This normalization procedure allows to assess the absolute transferred polarization to the aromatic spins and therefore to directly compare to numerical simulations. It defines the initial CO magnetization available for each contributing ^{13}CO-$^{13}C_{arom}$ spin pair as 1, distinguishing same spins with different distances as separate pairs. The resulting transferred polarization (and therefore the normalized signal integral) for each aromatic resonance appears as a sum of contributions from different spin pairs (e.g. for the $C\epsilon_{22}$ resonance, contributions from the spin pairs CO^1-$C\epsilon_{22}$ at 4.5 Å and CO^2-$C\epsilon_{22}$ at 5.0 Å and 5.5 Å), and can therefore exceed the theoretical maximum for a single spin pair.

2D ^{13}C-^{13}C DQ-SQ spectra

DQ-SQ 2D spectra were recorded with the pulse sequence shown in Fig. S2. All carbon pulses were centered close to the aromatic resonances (139 ppm). DQ excitation and reconversion of ^{13}C spins were achieved using S_3.[8] 100 kHz RF-field strength was used for heteronuclear decoupling using SW$_f$-TPPM[10,11] during indirect (t_1) and direct (t_2) detection periods, and CW[6] during S_3 recoupling. A *z*-filter of 100 µs was inserted before acquisition. Ten experiments were recorded with different mixing times ranging from 2 to 20 loops of S_3 for both the DQ excitation and reconversion blocks. Acquisition times were 30 and 9.2 ms in the direct and indirect dimension, respectively, using States-TPPI for quadrature detection.[12] 32 transients were accumulated for each of the 128 t_1 complex points, leading to a total experimental time of ~7.4 h. Prior to Fourier transform, data were zero-filled in both dimensions. No apodization was applied. Exceptionally, the spectrum in Fig. 4a was taken with 80 scans per complex point (instead of 32). This spectrum was not taken into account for the polarization buildup curves.

2D peak volume extraction

The Fourier transformed DQ-SQ 2D spectra were sheared by 45° prior to peak integration using a Monte-Carlo method.[13] The peak volumes were normalized as mentioned in the text and additionally scaled with respect to the CPMAS spectrum to take into account differential CP transfers.

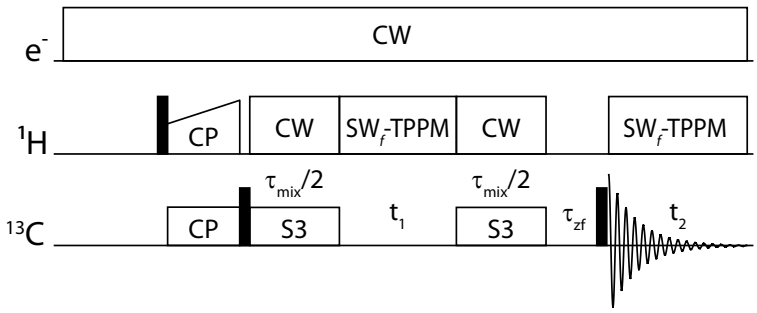

Fig. S2 Pulse sequence used for the acquisition of 2D DQ-SQ correlation spectra, employing the dipolar recoupling sequence S_3[8] for DQ excitation and reconversion. The S_3 pulse sequence can be expressed explicitly as $SR2_8^1 \equiv 360_{270}\,270_{90}\,90_{270}\,360_{90}\,270_{270}\,90_{90}\,360_{90}\,270_{270}\,90_{90}\,360_{270}\,270_{90}\,90_{270}$, with flip angles and RF-phases (subscripts) given in degrees. Filled bars denote π/2 pulses.

3) Influence of CSA tensor magnitude on the performance of common dipolar recoupling sequences

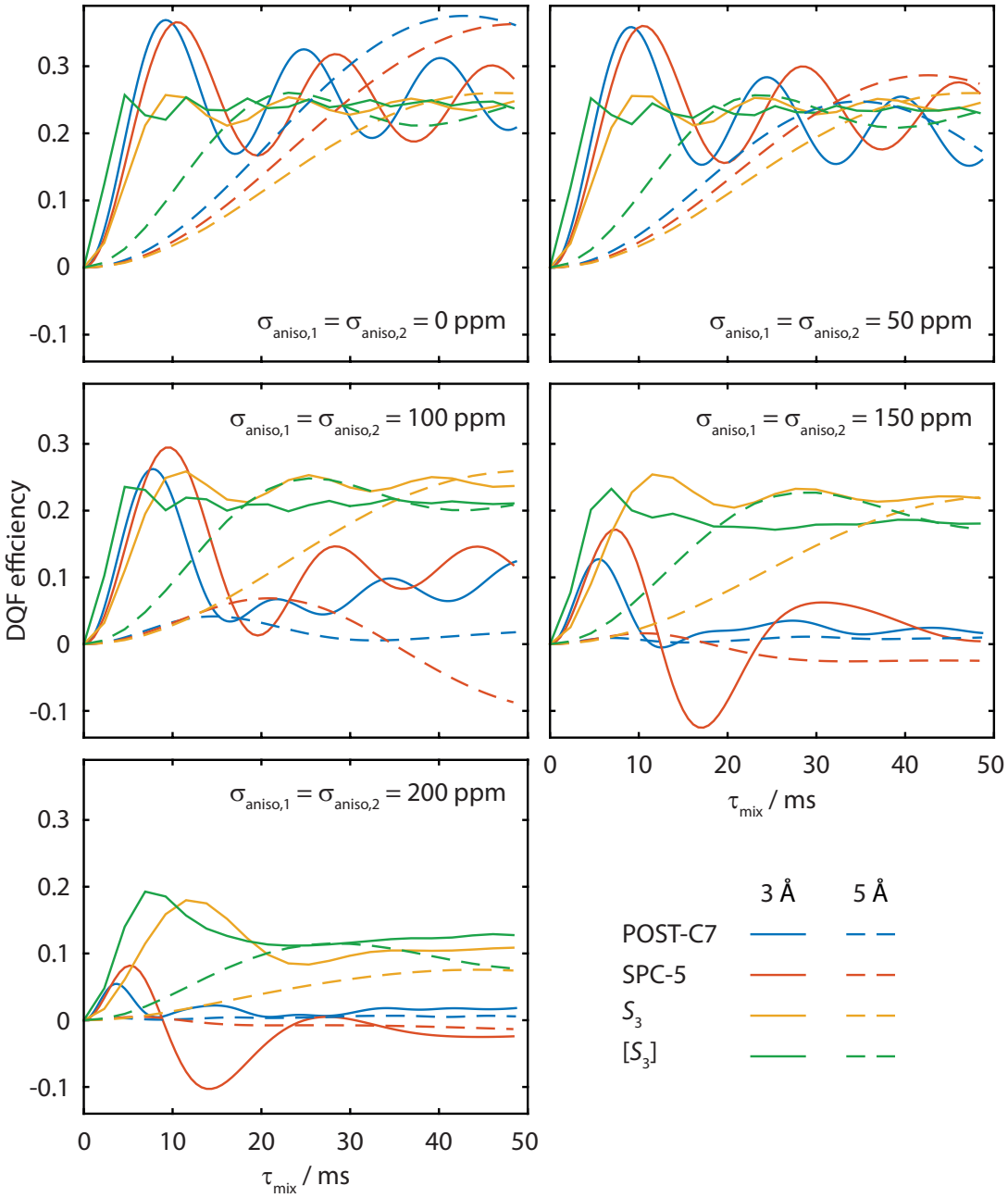

Fig. S3 SPINEVOLUTION[14] simulations of the performance of dipolar recoupling sequences POST-C7,[15] SPC-5,[16] S_3,[8] and $[S_3]$[8] in a double quantum filtered experiment with two carbon spins at internuclear distances of 3 Å (solid lines) or 5 Å (dashed lines). The different panels show the influence of increasing ^{13}C CSA magnitudes on both spins ($\sigma_{aniso,1}$, $\sigma_{aniso,2}$, see convention in Table S1), demonstrating the good performance of S_3 and $[S_3]$ under large CSA. Simulations were run at ν_r = 13.889 kHz.

4) Influence of CSA tensor properties on the performance of [S_3]

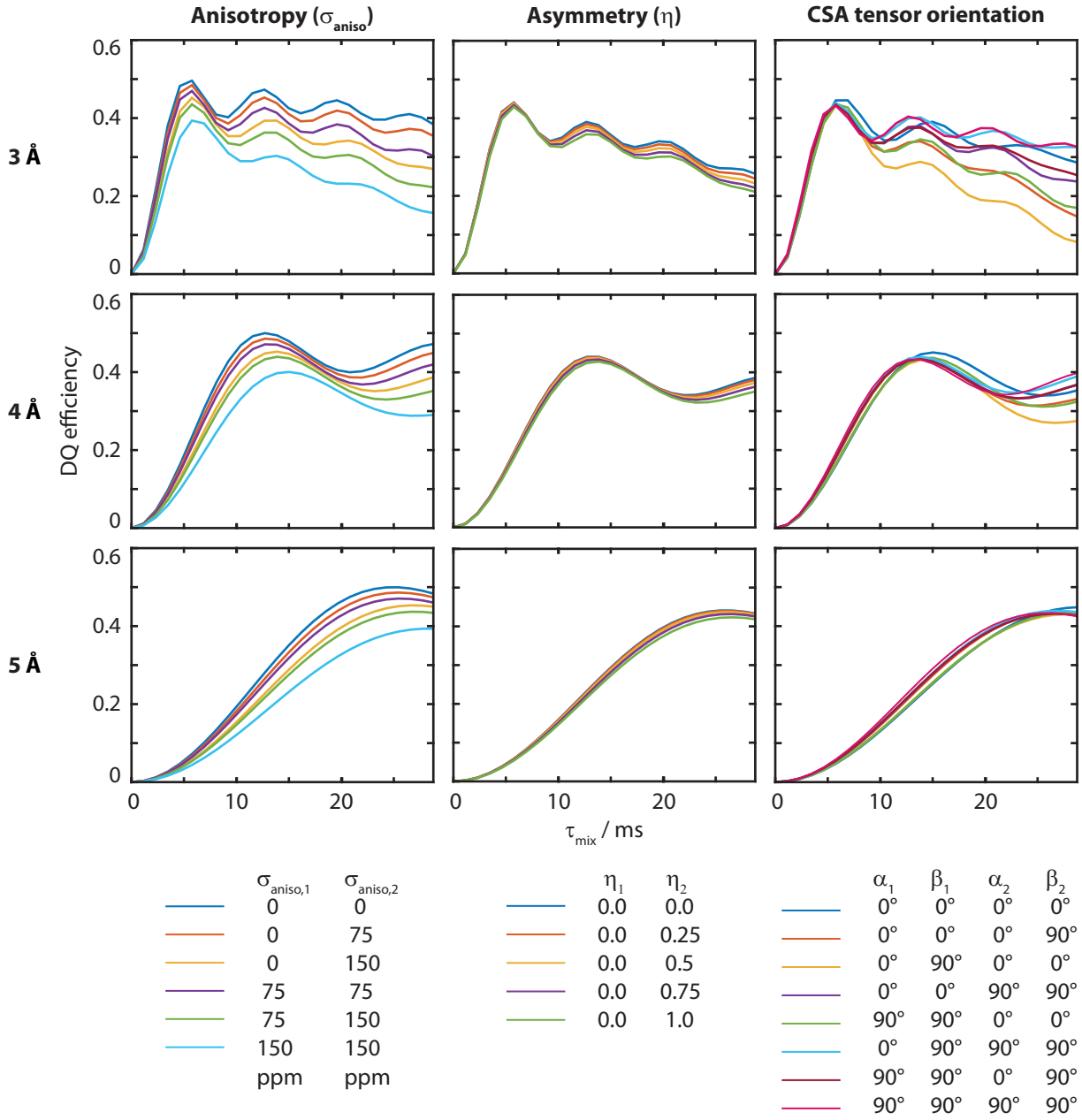

Fig. S4 SPINEVOLUTION[14] simulations of the performance of [S_3][8] in a dipolar recoupling experiment between two carbon spins as shown in Fig. 2, depending on the internuclear distance (rows; 3 Å, 4 Å, 5 Å), and the anisotropy (σ_{aniso}), the asymmetry (η, see convention in Table S1 for σ_{aniso} and η) and the orientation of the CSA tensor (columns). The tensor orientation, in the principle axis frame, is described by the Euler angles α, β and γ, as used in the SPINEVOLUTION software. If not given otherwise in the legends, the following parameters were used in all simulations: ν_r = 13.889 kHz, $\sigma_{aniso,1}$ = 75 ppm, $\sigma_{aniso,2}$ = 150 ppm, η_1 = 1.0, η_2 = 0.6, α_1 = 0°, β_1 = 30°, γ_1 = 40°, α_2 = 20°, β_2 = 80°, γ_2 = 10°.

5) Influence of CSA tensor properties on the performance of S_3

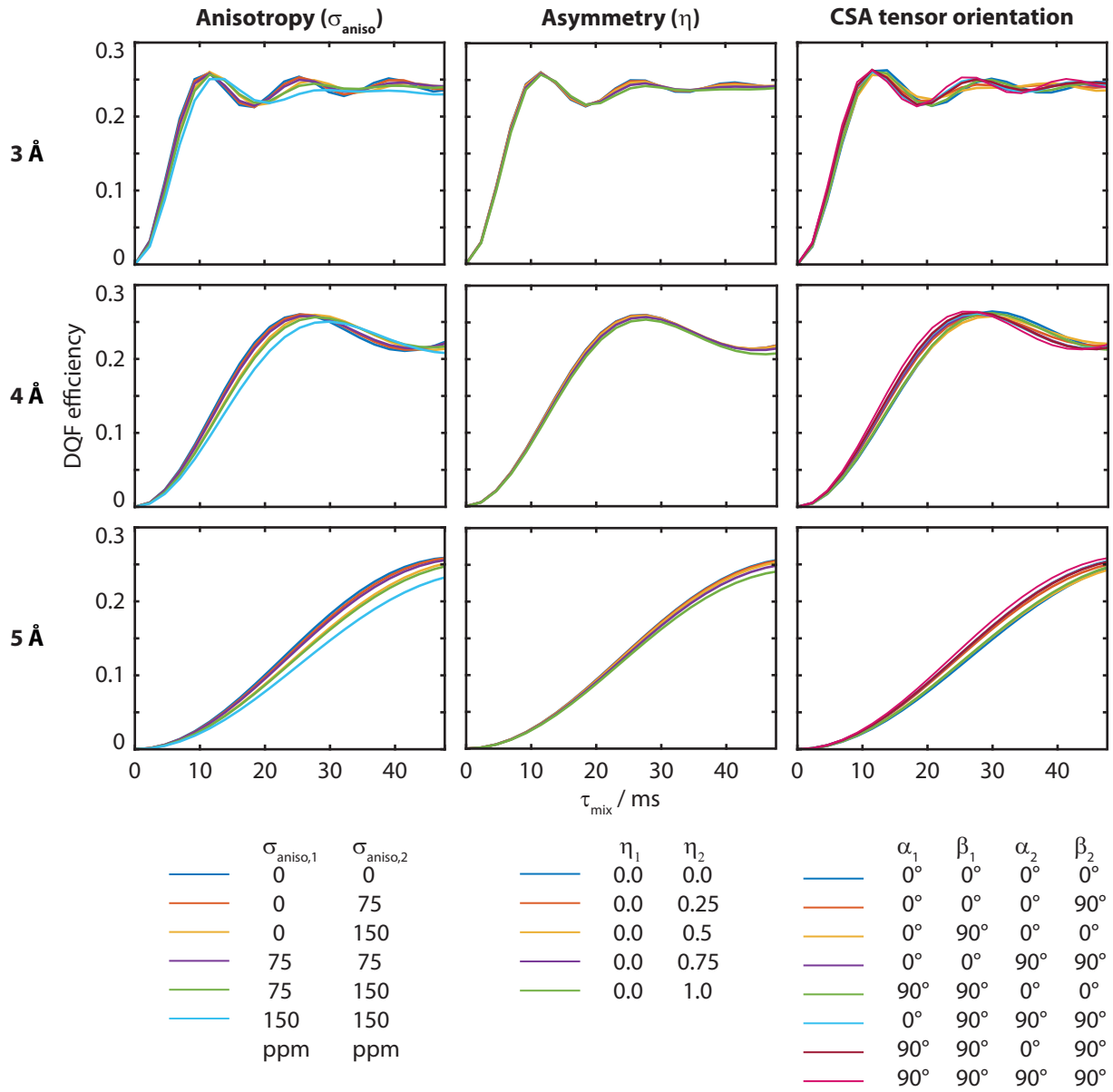

Fig. S5 SPINEVOLUTION[14] simulations of the performance of S_3[8] in a double quantum filtered dipolar recoupling experiment between two carbon spins as employed for spectra in Fig. 4, depending on the internuclear distance (rows; 3 Å, 4 Å, 5 Å), and the anisotropy (σ_{aniso}), the asymmetry (η, see convention in Table S1 for σ_{aniso} and η) and the orientation of the CSA tensor (columns). The tensor orientation is described by the Euler angles α, β and γ, as used in the SPINEVOLUTION software. If not given otherwise in the legends, the following parameters were used in all simulations: ν_r = 13.889 kHz, $\sigma_{aniso,1}$ = 75 ppm, $\sigma_{aniso,2}$ = 150 ppm, η_1 = 1.0, η_2 = 0.6, α_1 = 0°, β_1 = 30°, γ_1 = 40°, α_2 = 20°, β_2 = 80°, γ_2 = 10°.

6) Impact of the “cutoff distance” on the fitting quality of experimental buildups at NA

Fig. S6 complements Fig. 3 and presents a detailed analysis of the impact of the cutoff distance used to simulate polarization transfer on the analysis of experimental buildups. It reports the minimized RMSD (red) as well as the corresponding *A* values (black solid line) and their deviation from unity (|1 - *A*|, black dotted line) for cutoff distances between 3 and 15 Å, determined for the experimental data obtained with the 1D approach.

Starting from 3 Å and upon inclusion of longer distances, the RMSD first decreases significantly until it reaches a minimum and then increases again. Similarly, the *A* value decreases from a value much larger than 1 to a value smaller than 1. For a given peak, the RMSD and the |1 - *A*| curves reach a minimum at roughly the same cutoff distance, meaning that the lowest RMSD does coincide with an *A* value very close to 1. This remarkable observation demonstrates that the experimental data can be reproduced very well by simulation, justifying our way of modeling/fitting the experimental data.

The exact positions of the RMSD minima depend on the peak and occur at a cutoff distance between 5.5 and 7.5 Å. This confirms our assumption that the experiments are sensitive to long distances (> 4.5 Å), and that they therefore have to be included in simulations. At the same time, too long distances cannot be observed due to dipolar truncation which yields an increase of the RMSD. The slightly different positions of the minima in the 6 cases considered here can be explained by the different numbers and lengths of contributing distances. When considering spin pairs at distances between 5 and 7 Å, some of them are in proximity of a third ^{13}C spin and hence the polarization transfer is affected by dipolar truncation, whereas others are still isolated. Therefore, such distances do still contribute to the buildup curves, but with a lowered intensity. Depending on how many distances fall in this category, the “optimum” cutoff distance can change, and the corresponding *A* value may not be exactly unity. This justifies the determination of different *A* values for each peak in order to obtain the best fit. It can also be seen that 7 Å is a reasonable choice for a cutoff distance. Slightly different cutoffs, however, could also be considered and would still lead to good fitting results.

The normalization of experimental data with respect to the polarization transfer is an immense advantage of these experiments because it provides a second estimate (apart from the RMSD) for the quality of fitting, since *A* should be close to 1. This will be of great importance for *de novo* fitting of such buildup curves, since not only an RMSD has to be minimized, but also a reasonable *A* value has to be found.

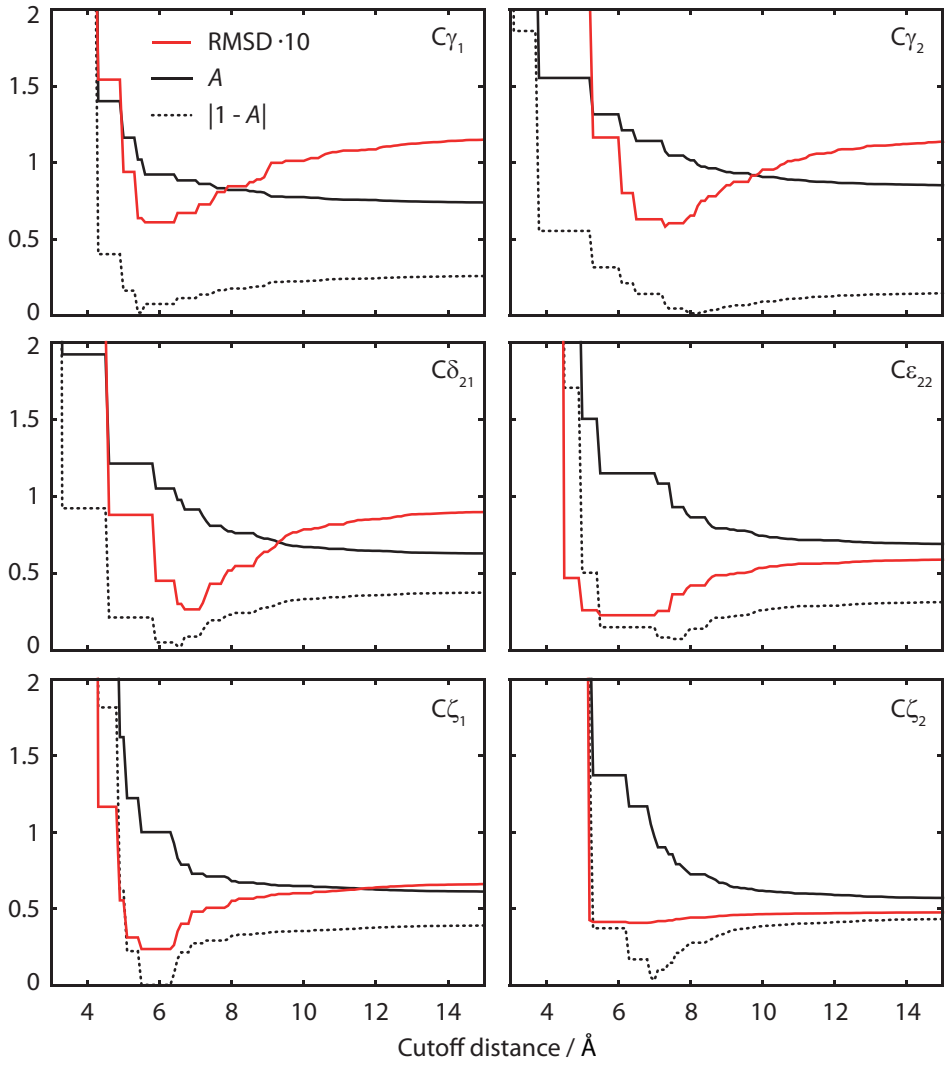

Fig. S6 Quality of the fit of simulated buildup curves to experimental data from the 1D approach (see Fig. 2), depending on the maximum distance (cutoff distance) included in the simulations. For these plots, simulations for all relevant spin pairs with distances up to the respective cutoff distance were summed up and fitted to the experimental data with the amplitude factor *A* by minimizing the RMSD between experiment and simulation. The corresponding RMSD (red solid line) and *A* value (black solid line) are plotted here depending on the cutoff distance.

7) Prediction of the molecular conformation

The molecular mechanics software TINKER[17] (version 7.1) was used for conformational search of the potential energy surface of one cyclo-FF molecule, employing the AMBER99 force field.[18] Six local minima were found. Their geometries were refined using DFT-based geometry optimization as implemented in the ORCA software package (version 3.0.2).[19] The optimizations were done in two steps, first using the TZVP basis set[20] and the BP86 functional,[21,22] and subsequently with the def2-TZVP basis set[20,23] and the B3LYP hybrid functional,[24–26] including atom-pairwise dispersion correction with Becke-Johnson damping (DFT-D3).[27,28] CSA tensors of ^{13}C were computed for the three lowest energy structures (shown in Fig. 7 and again in Fig. S7) using the IGLO-III basis set[29] and the B3LYP functional.

For a qualitative comparison with the experimental data from the 1D approach presented in the paper, the expected polarization buildup curves for these three geometries were simulated with SPINEVOLUTION.[14] The same settings as given in the experimental section were used, taking into account the relevant intramolecular spin pairs and the ^{13}C CSAs as computed with ORCA. Fig. S7 shows these simulations, plotted together with the experimental points. The $C\delta_{21}$ and $C\epsilon_{22}$ buildups are omitted because the particular δ_{21} and ϵ_{22} carbons cannot be assigned in these structures.

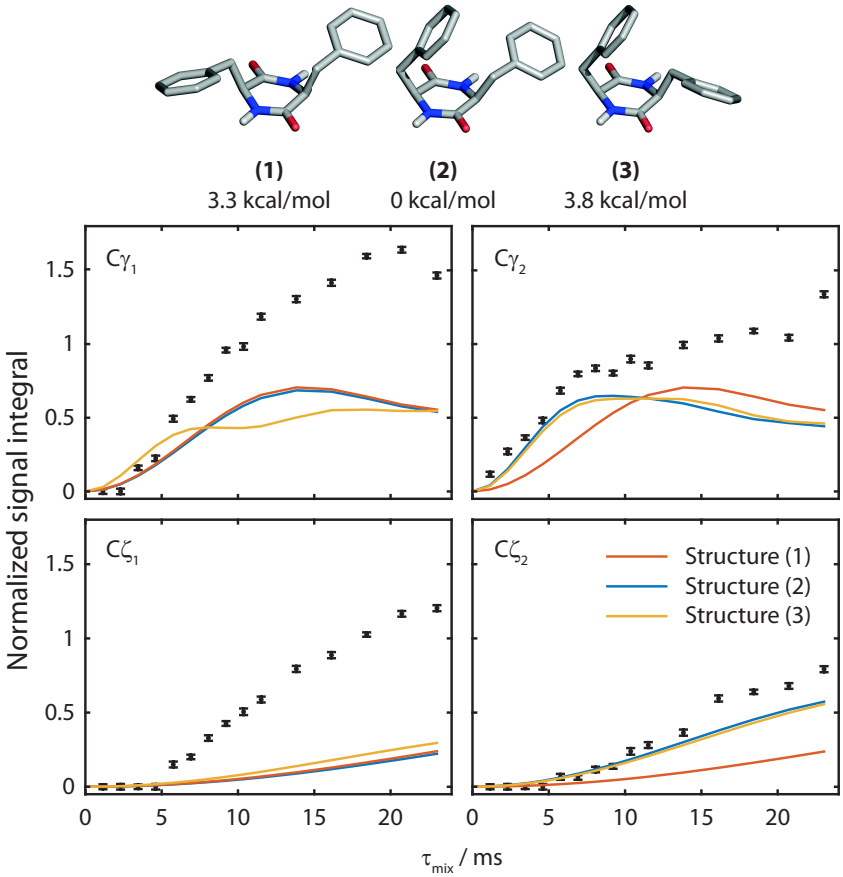

Fig. S7 Top: The three lowest energy structures of cyclo-FF and their relative energies as obtained after conformational search and subsequent geometry optimization by DFT. Bottom: Experimental data points (black) from the 1D approach and simulated polarization buildup curves for structures (1) - (3). Since only the molecular structure was optimized and not the crystal packing, only intramolecular spin pairs could be included in the simulation. No scaling was applied to the simulated data.

References

1 C. J. Pickard and F. Mauri, *Phys. Rev. B*, 2001, **63**, 245101–245113.

2 P. Giannozzi, S. Baroni, N. Bonini, M. Calandra, R. Car, C. Cavazzoni, D. Ceresoli, G. L. Chiarotti, M. Cococcioni, I. Dabo, A. Dal Corso, S. de Gironcoli, S. Fabris, G. Fratesi, R. Gebauer, U. Gerstmann, C. Gougoussis, A. Kokalj, M. Lazzeri, L. Martin-Samos, N. Marzari, F. Mauri, R. Mazzarello, S. Paolini, A. Pasquarello, L. Paulatto, C. Sbraccia, S. Scandolo, G. Sclauzero, A. P. Seitsonen, A. Smogunov, P. Umari and R. M. Wentzcovitch, *J. Phys. Condens. Matter*, 2009, **21**, 395502.

3 M. Gdaniec and B. Liberek, *Acta Crystallogr. Sect. C Cryst. Struct. Commun.*, 1986, **42**, 1343–1345.

4 U. Haeberlen, *High Resolution NMR in Solids, Selective Averaging*, Academic Press, New York, 1976.

5 F. Delaglio, S. Grzesiek, G. Vuister, G. Zhu, J. Pfeifer and A. Bax, *J. Biomol. NMR*, 1995, **6**, 277–293.

6 A. Bloom and J. Shoolery, *Phys. Rev.*, 1955, **97**, 1261–1265.

7 B. M. Fung, A. K. Khitrin and K. Ermolaev, *J. Magn. Reson.*, 2000, **142**, 97–101.

8 G. Teymoori, B. Pahari, B. Stevensson and M. Edén, *Chem. Phys. Lett.*, 2012, **547**, 103–109.

9 H. Geen and R. Freeman, *J. Magn. Reson.*, 1991, **93**, 93–141.

10 R. Thakur, N. Kurur and P. Madhu, *Chem. Phys. Lett.*, 2006, **426**, 459–463.

11 S. Paul, N. D. Kurur and P. K. Madhu, *J. Magn. Reson.*, 2010, **207**, 140–148.

12 D. Marion, M. Ikura, R. Tschudin and A. Bax, *J. Magn. Reson.*, 1989, **85**, 393–399.

13 R. Romano, D. Paris, F. Acernese, F. Barone and A. Motta, *J. Magn. Reson.*, 2008, **192**, 294–301.

14 M. Veshtort and R. G. Griffin, *J. Magn. Reson.*, 2006, **178**, 248–282.

15 M. Hohwy, H. J. Jakobsen, M. Edén, M. H. Levitt and N. C. Nielsen, *J. Chem. Phys.*, 1998, **108**, 2686–2694.

16 M. Hohwy, C. M. Rienstra, C. P. Jaroniec and R. G. Griffin, *J. Chem. Phys.*, 1999, **110**, 7983–7992.

17 J. W. Ponder and F. M. Richards, *J. Comput. Chem.*, 1987, **8**, 1016–1024.

18 J. Wang, P. Cieplak and P. A. Kollman, *J. Comput. Chem.*, 2000, **21**, 1049–1074.

19 F. Neese, *Wiley Interdiscip. Rev. Comput. Mol. Sci.*, 2012, **2**, 73–78.

20 A. Schäfer, H. Horn and R. Ahlrichs, *J. Chem. Phys.*, 1992, **97**, 2571–2577.

21 J. P. Perdew, *Phys. Rev. B*, 1986, **33**, 8822–8824.

22 A. D. Becke, *Phys. Rev. A*, 1988, **38**, 3098–3100.

23 F. Weigend and R. Ahlrichs, *Phys. Chem. Chem. Phys.*, 2005, **7**, 3297–3305.

24 C. Lee, W. Yang and R. G. Parr, *Phys. Rev. B*, 1988, **37**, 785–789.

25 A. D. Becke, *J. Chem. Phys.*, 1993, **98**, 5648–5653.

26 P. J. Stephens, F. J. Devlin, C. F. Chabalowski and M. J. Frisch, *J. Phys. Chem.*, 1994, **98**, 11623–11627.

27 S. Grimme, J. Antony, S. Ehrlich and H. Krieg, *J. Chem. Phys.*, 2010, **132**, 154104–154119.

28 S. Grimme, S. Ehrlich and L. Goerigk, *J. Comput. Chem.*, 2011, **32**, 1456–1465.

29 W. Kutzelnigg, U. Fleischer and M. Schindler, Springer-Verlag, Berlin, Heidelberg, 1990, vol. 23, pp. 165–262.